EFFECTS OF TOPOGRAPHY ON PROPAGATION AND DEVELOPMENT OF INERTIA GRAVITY WAVE

Wang Xingbao (王兴宝)

Institute of Meteorology. PLA Air Force. Nanjing 211101

Received July 28, 1994; revised January 9, 1995

ABSTRACT

Effects of topography on the propagation and development of inertia gravity waves are investigated by means of WKBJ method. The equation of wave action conservation is obtained. It is found that the inertia gravity wave tends to propagate to the higher elevation area, meanwhile the amplitudes of the waves increase. While the inertia gravity waves propagate to a lower elevation area, their amplitudes decrease.

Key words: topography, inertia gravity wave, WKBJ method

I. INTRODUCTION

It is recognized that the influence of inertia gravity waves on weather variation is of significance along with the advances of atmospheric probing technology. The field of clouds and precipitation is modulated by inertia gravity waves. Some convective storms are triggered by inertia gravity waves as the atmosphere is under the latent instability condition and so on. Many theoretical investigations about the development of inertia gravity wave and its relation with convection have been carried out. Chao (1980), Liu and Liu (1987), He (1989) and Wu (1990) investigated the effect of non-uniform stratification on the development of inertia gravity waves and tried to find out the relations between the convection and storm rainfall. Sun and Zhao (1989) studied the effect of the baroclinic basic flow on a paralleled mesoscale disturbance development. Wang and Zhou (1994) discussed the development of mesoscale transversal wave disturbance on the pure baroclinic flow. Wang and Zhang (1992; 1993) examined the development of inertia gravity wave packet superposed on the three-dimensional non-uniform flow in a non-uniform stratified atmosphere. Some interesting results have been obtained. But it must be recognized that the external forcing conditions, such as topography and diabatic heating, are also important to the development of inertia gravity waves, besides the influences of internal structure of atmosphere on the development of inertia gravity waves. Topography can not only excite inertia gravity waves but also affect the development and propagation of inertia gravity waves. There have been many researches on the effects of topography on gravity waves in oceanography and water dynamics fields. But there is few work about the effects of topography on the atmospheric inertia gravity waves. Lu (1986) discussed the effect of topography on the stability of inertia gravity waves on the low level geostrophic flow. Wu (1994) discussed the effect of topography only with the north-south oriented slope ($\partial/\partial x=0$) on the inertia gravity waves. He also assumed that the wavelength

in west-east is infinite. So the result is very limited. In the real atmosphere the height of topography varies two-dimensionally ($h_B = h_B(x, y)$). The wave motion is dependent on x and y components. It is more useful to study the development and propagation of inertia gravity waves on two-dimensionally varying topography. This paper will discuss the said problem.

II. BASIC EQUATIONS

In order to deal with the effect of topography easily, consider the two-layer fluid model. Assume that the fluid density in the upper layer is ρ_1 and that in the lower layer is ρ_2. ρ_1 and ρ_2 are constant. So the equations governing the lower layer fluid motion are

$$\begin{aligned} &\frac{\partial u}{\partial t} + u\frac{\partial u}{\partial x} + v\frac{\partial u}{\partial y} - fv = -g^*\frac{\partial h}{\partial x}, \\ &\frac{\partial v}{\partial t} + u\frac{\partial v}{\partial x} + v\frac{\partial v}{\partial y} + fu = -g^*\frac{\partial h}{\partial y}, \\ &\frac{\partial h}{\partial t} + \frac{\partial}{\partial x}[(h-h_B)u] + \frac{\partial}{\partial y}[(h-h_B)v] = 0, \end{aligned} \tag{1}$$

where $g^* = (\rho_2 - \rho_1)\, g/\rho_2$, $h_B = h_B(x, y)$ are reduced gravity and the height of topography respectively. And h is the height of interface of the two fluids. In the static state case,

$$u = v = 0, \qquad h = H_0. \tag{2}$$

Superpose small perturbations u', v', h' on Eq. (2), then

$$u = u', \qquad v = v', \qquad h = H_0 + h'. \tag{3}$$

Substituting Eq. (3) into Eq. (1) by neglecting all terms which are nonlinear in the perturbation, we obtain the linear perturbation equations:

$$\begin{aligned} &\frac{\partial u}{\partial t} - fv = -\frac{\partial \varphi}{\partial x}, \\ &\frac{\partial v}{\partial t} + fu = -\frac{\partial \varphi}{\partial y}, \\ &\frac{\partial \varphi}{\partial t} + \Phi\left(\frac{\partial u}{\partial x} + \frac{\partial v}{\partial y}\right) - u\frac{\partial \varphi_B}{\partial x} - v\frac{\partial \varphi_B}{\partial y} = 0, \end{aligned} \tag{4}$$

where "$'$" has been omitted and $\varphi = g^* h'$, $\Phi = g^*(H_0 - h_B)$, $\varphi_B = g^* h_B$. Eq. (4) is used to study the effect of topography on the inertia gravity waves.

III. WKBJ ANALYSIS AND WAVE PACKET GOVERNING EQUATIONS

Assume that topography height $h_B(x, y)$ is a slowly varying function of (x, y). The perturbation wavelength L satisfies $|\nabla h_B| / (h_B/L) = \varepsilon \ll 1$. So a slow time T and enlarged coordinate (X, Y) can be introduced as follows:

$$X = \varepsilon x, \qquad Y = \varepsilon y, \qquad T = \varepsilon t. \tag{5}$$

Assume that Eq. (4) has a wave packet solution as follows:

$$u = \hat{u}\exp\left(\frac{i\theta}{\varepsilon}\right), \quad v = \hat{v}\exp\left(\frac{i\theta}{\varepsilon}\right), \quad \varphi = \hat{\varphi}\exp\left(\frac{i\theta}{\varepsilon}\right), \tag{6}$$

$\hat{u}$, $\hat{v}$, $\hat{\varphi}$ are the function of X, Y, T. θ is a phase function and satisfies

$$\frac{\partial \theta}{\partial X} = k, \quad \frac{\partial \theta}{\partial Y} = l, \quad \frac{\partial \theta}{\partial T} = -\sigma, \tag{7}$$

where k, l are the local wavenumbers along X, Y; σ is the instantaneous local frequency. k, l,

σ are also slowly varying functions of x, y, t. So the following relations can be obtained:

$$\frac{\partial k}{\partial Y} = \frac{\partial l}{\partial X}, \quad \frac{\partial k}{\partial T} = -\frac{\partial \sigma}{\partial X}, \quad \frac{\partial l}{\partial T} = -\frac{\partial \sigma}{\partial Y}. \tag{8}$$

With WKBJ approximation, the asymptotic expansion of $\hat{u}$, $\hat{v}$, $\hat{\varphi}$ can be written as

$$\begin{aligned} \hat{u} &= u_0 + \varepsilon u_1 + \varepsilon^2 u_2 + \cdots, \\ \hat{v} &= v_0 + \varepsilon v_1 + \varepsilon^2 v_2 + \cdots, \\ \hat{\varphi} &= \varphi_0 + \varepsilon \varphi_1 + \varepsilon^2 \varphi_2 + \cdots. \end{aligned} \tag{9}$$

Substituting Eqs. (6)—(9) into Eq. (4) and expanding every term into a power series of ε, we obtain the following zero-order equations:

$$\begin{aligned} -i\sigma u_0 - f v_0 + ik\varphi_0 &= 0, \\ -i\sigma v_0 + f u_0 + il\varphi_0 &= 0, \\ -i\sigma\varphi_0 + \Phi\,(iku_0 + ilv_0) &= 0. \end{aligned} \tag{10}$$

From (10) we obtain $-i\sigma\,(\sigma^2 - f^2)\varphi_0 + i\sigma\Phi\,(k^2 + l^2)\varphi_0 = 0$. If $\varphi_0 \neq 0$, then

$$\sigma[\sigma^2 - f^2 - (k^2 + l^2)\Phi] = 0,$$

i. e.

$$\sigma = 0 \quad \text{or} \quad \sigma^2 = f^2 + (k^2 + l^2)\Phi. \tag{11}$$

$\sigma = 0$ is the dispersion relation corresponding to vortex slow waves which will not be discussed here. Note that $\sigma^2 = f^2 + (k^2 + l^2)\Phi$ is the dispersion relation corresponding to inertia gravity waves, so $\sigma = \pm\sqrt{f^2 + (k^2 + l^2)\Phi} = \sigma\,(X, Y, T)$ and the components of the group velocity are given by

$$\begin{aligned} C_{gX} &= \frac{\partial \sigma}{\partial k} = \frac{k}{\sigma}\Phi, \\ C_{gY} &= \frac{\partial \sigma}{\partial l} = \frac{l}{\sigma}\Phi, \end{aligned} \tag{12}$$

and the components of the phase velocity are given by

$$\begin{aligned} C_x &= \frac{\sigma}{k} = \frac{\sigma^2}{k^2\Phi} C_{gX}, \\ C_y &= \frac{\sigma}{l} = \frac{\sigma^2}{l^2\Phi} C_{gY}. \end{aligned} \tag{13}$$

From Eqs. (8), (11) and (12), the kinematic relations can be written as

$$\begin{aligned} \frac{D_g k}{DT} &= -\left(\frac{\partial \sigma}{\partial X}\right)_{(Y, T, k, l)} = -\frac{(k^2 + l^2)}{2\sigma}\frac{\partial \Phi}{\partial X} = \frac{(k^2 + l^2)}{2\sigma}\frac{\partial \varphi_B}{\partial X}, \\ \frac{D_g l}{DT} &= -\left(\frac{\partial \sigma}{\partial Y}\right)_{(X, T, k, l)} = -\frac{(k^2 + l^2)}{2\sigma}\frac{\partial \Phi}{\partial Y} = \frac{(k^2 + l^2)}{2\sigma}\frac{\partial \varphi_B}{\partial Y}, \\ \frac{D_g \sigma}{DT} &= \left(\frac{\partial \sigma}{\partial T}\right)_{(X, Y, k, l)} = 0, \end{aligned} \tag{14}$$

where

$$\frac{D_g}{DT} = \frac{\partial}{\partial T} + C_{gX}\frac{\partial}{\partial X} + C_{gY}\frac{\partial}{\partial Y}. \tag{15}$$

From Eqs. (11) and (10) we get

$$\begin{aligned} u_0 &= \frac{(\sigma k + ilf)}{(\sigma^2 - f^2)}\varphi_0 = a\varphi_0 = a_r\varphi_0 + ia_i\varphi_0, \\ v_0 &= \frac{(\sigma l - ikf)}{(\sigma^2 - f^2)}\varphi_0 = b\varphi_0 = b_r\varphi_0 + ib_i\varphi_0, \end{aligned} \tag{16}$$

thus

$$a_r = \frac{\sigma k}{(\sigma^2 - f^2)}, \qquad b_r = \frac{\sigma l}{(\sigma^2 - f^2)},$$
$$a_i = \frac{lf}{(\sigma^2 - f^2)}, \qquad b_i = -\frac{kf}{(\sigma^2 - f^2)}. \tag{16'}$$

Secondly, we obtain the following first-order equations:

$$\begin{aligned}
&-i\sigma u_1 - fv_1 + ik\varphi_1 = -\frac{\partial u_0}{\partial T} - \frac{\partial \varphi_0}{\partial X} = A,\\
&-i\sigma v_1 + fu_1 + il\varphi_1 = -\frac{\partial v_0}{\partial T} - \frac{\partial \varphi_0}{\partial Y} = B,\\
&-i\sigma\varphi_1 + \Phi(iku_1 + ilv_1) = -\frac{\partial \varphi_0}{\partial T} - \Phi\left(\frac{\partial u_0}{\partial X} + \frac{\partial v_0}{\partial Y}\right)\\
&\qquad + \left(u_0\frac{\partial \varphi_B}{\partial X} + v_0\frac{\partial \varphi_B}{\partial Y}\right) = C.
\end{aligned} \tag{17}$$

From Eq. (17) and dispersion relation of Eq. (11) we have

$$\frac{\Phi}{(f^2 - \sigma^2)}[(\sigma k - ifl)A + (\sigma l + ifk)B] - C = 0. \tag{18}$$

Using Eqs. (11), (12), (16) and substituting A, B, C of (17) into (18) result in

$$\begin{aligned}
&\frac{D_g\varphi_0}{DT} + \frac{(\sigma^2 - f^2)}{2\sigma^2}\left\{\frac{\Phi}{(f^2 - \sigma^2)}\left[-(\sigma k - ifl)\frac{\partial a}{\partial T} - (\sigma l + ifk)\frac{\partial b}{\partial T}\right]\right.\\
&\qquad \left. + \Phi\left(\frac{\partial a}{\partial X} + \frac{\partial b}{\partial Y}\right) - a\frac{\partial \varphi_B}{\partial X} - b\frac{\partial \varphi_B}{\partial Y}\right\}\varphi_0 = 0.
\end{aligned} \tag{19}$$

Let $\varphi_0 = |\varphi_0|\exp(i\alpha)$ and substitute it into Eq. (19) and separate Eq. (19) into its real part and imaginary part. After some deduction, we have

$$\frac{D_g\varphi_0}{DT} = \exp(i\alpha)\frac{D_g|\varphi_0|}{DT} + i|\varphi_0|\exp(i\alpha)\frac{D_g\alpha}{DT}$$

and

$$\begin{aligned}
&\frac{D_g|\varphi_0|}{DT} + \frac{(\sigma^2 - f^2)}{2\sigma^2}\left[\frac{\Phi}{(\sigma^2 - f^2)}\left(\sigma k\frac{\partial a_r}{\partial T} + fl\frac{\partial a_i}{\partial T} + \sigma l\frac{\partial b_r}{\partial T} - fk\frac{\partial b_i}{\partial T}\right)\right.\\
&\qquad \left. + \Phi\left(\frac{\partial a_r}{\partial X} + \frac{\partial b_r}{\partial Y}\right) - a_r\frac{\partial \varphi_B}{\partial X} - b_r\frac{\partial \varphi_B}{\partial Y}\right]|\varphi_0| = 0,
\end{aligned} \tag{20}$$

$$\begin{aligned}
&\frac{D_g\alpha}{DT} + \frac{(\sigma^2 - f^2)}{2\sigma^2}\left[\frac{\Phi}{(\sigma^2 - f^2)}\left(\sigma k\frac{\partial a_i}{\partial T} - fl\frac{\partial a_r}{\partial T} + \sigma l\frac{\partial b_i}{\partial T} + fk\frac{\partial b_r}{\partial T}\right)\right.\\
&\qquad \left. + \Phi\left(\frac{\partial a_i}{\partial X} + \frac{\partial b_i}{\partial Y}\right) - a_i\frac{\partial \varphi_B}{\partial X} - b_i\frac{\partial \varphi_B}{\partial Y}\right] = 0.
\end{aligned} \tag{21}$$

Inserting (16') into Eqs. (20) and (21) and using relations of Eqs. (8), (11) and (12), after carefully manipulation we obtain

$$\frac{D_g|\varphi_0|^2}{DT} + |\varphi_0|^2\nabla\cdot\boldsymbol{C}_g = 0,$$

or

$$\frac{\partial|\varphi_0|^2}{\partial T} + \nabla\cdot(|\varphi_0|^2\boldsymbol{C}_g) = 0, \tag{22}$$

and

$$\frac{D_g\alpha}{DT} - \frac{f}{2\sigma^2}\left(l\frac{\partial \varphi_B}{\partial X} - k\frac{\partial \varphi_B}{\partial Y}\right) = 0. \tag{23}$$

Since α is the phase function of wave train envelope, Eq. (24) describes the variation of phase function following the wave packet. If $f=0$ or $\varphi_B=0$, then $D_g\alpha/DT=0$, namely

$$\alpha(X, Y, T) = \alpha(X - C_{gX}T, Y - C_{gY}T) = \alpha(\boldsymbol{r} - \boldsymbol{C}_g), \tag{24}$$

which states that the wave packet propagates at the local group velocity. In the atmosphere, $f\sim10^{-4}\ \mathrm{s}^{-1}$ and if assuming that the topography varies slowly, then $D_g\alpha/DT\approx 0$. That is to say the hypothesis that wave packet propagates at the local group velocity is approximately satisfied.

Here the physical implication of Eq. (23) is to be discussed emphatically. The average kinetic energy and perturbation potential energy over a period and a wavelength contained in a column of unit horizontal cross section (i. e. energy density) are respectively as follows:

$$KE = \frac{1}{2}\rho_2\overline{\int_{h_B}^{h}(u^2+v^2)\mathrm{d}z} = \frac{1}{2}\rho_2\overline{(H_0+h-h_B)(u^2+v^2)}, \tag{25}$$

$$PE = \overline{\int_{h_B}^{h}(\rho_2 g^* z)\mathrm{d}z} - \overline{\int_{h_B}^{H_0}\rho_2 g^* z\,\mathrm{d}z} = \frac{1}{2}\rho_2 g^*\overline{(h^2-H_0{}^2)}, \tag{26}$$

where $\overline{(\ )} = \int_0^T\int_0^{2\pi/k}\int_0^{2\pi/l}(\ )\,\mathrm{d}x\,\mathrm{d}y\,\mathrm{d}t\,/\,[T\,(2\pi/k)\,(2\pi/l)]$. Using Eqs. (6) and (9) and neglecting the $O(\varepsilon)$ and higher order small terms, we obtain

$$u = u_0\exp\left(\frac{i\theta}{\varepsilon}\right),\quad v = v_0\exp\left(\frac{i\theta}{\varepsilon}\right),\quad \varphi = \varphi_0\exp\left(\frac{i\theta}{\varepsilon}\right). \tag{27}$$

Inserting Eq. (27) into Eqs. (25) and (26), considering $(H_0-h_b)\gg h'$, then

$$KE = \frac{\rho_2\Phi(|u_0|^2+|v_0|^2)}{4g^*}, \tag{28}$$

$$PE = \frac{\rho_2|\varphi_0|^2}{4g^*}. \tag{29}$$

According to Eq. (16), Eq. (28) may be rewritten as

$$KE = \rho_2\frac{(\sigma^2+f^2)}{(\sigma^2-f^2)}\frac{|\varphi_0|^2}{4g^*}, \tag{28'}$$

then the total perturbation energy density is

$$E = KE + PE = \rho_2\frac{\sigma^2}{(\sigma^2-f^2)}\frac{|\varphi_0|^2}{2g^*}. \tag{30}$$

From $(D_g\sigma)/(DT) = 0$ (see Eq. (14)) and Eq. (23) we have

$$\begin{aligned}
&\frac{\partial}{\partial T}\left(\frac{\sigma^2}{\sigma^2-f^2}|\varphi_0|^2\right) + \nabla\cdot\left(\frac{\sigma^2}{\sigma^2-f^2}|\varphi_0|^2\boldsymbol{C}_g\right) = 0,\\
&\frac{\partial}{\partial T}\left(\frac{\sigma^2+f^2}{\sigma^2-f^2}|\varphi_0|^2\right) + \nabla\cdot\left(\frac{\sigma^2+f^2}{\sigma^2-f^2}|\varphi_0|^2\boldsymbol{C}_g\right) = 0,\\
&\frac{\partial}{\partial T}(|\varphi_0|^2) + \nabla\cdot(|\varphi_0|^2\boldsymbol{C}_g) = 0,
\end{aligned} \tag{31}$$

$\frac{\sigma^2}{\sigma^2-f^2}|\varphi_0|^2$, $\frac{\sigma^2+f^2}{\sigma^2-f^2}|\varphi_0|^2$ and $|\varphi_0|^2$ can be defined as generalized wave actions of inertia gravity waves. From Eqs. (28′), (29) and (30), integrating Eq. (31) over the volume V occupied by whole wave packet gives

$$\frac{\partial}{\partial T}\iiint_V E\,\mathrm{d}\tau = 0,$$
$$\frac{\partial}{\partial T}\iiint_V KE\,\mathrm{d}\tau = 0, \tag{32}$$
$$\frac{\partial}{\partial T}\iiint_V PE\,\mathrm{d}\tau = 0.$$

Eq. (32) indicates that the sum of kinetic energy and perturbation potential energy is conserved. The kinetic energy and perturbation potential energy are conserved individually. There is no conversion between the kinetic energy and perturbation potential energy. In fact Eqs. (28′), (29) and (30) show that the proportions between every two of them are given by

$$\frac{E}{PE} = \frac{2\sigma^2}{\sigma^2 - f^2},$$
$$\frac{E}{KE} = \frac{2\sigma^2}{\sigma^2 + f^2}, \tag{33}$$
$$\frac{KE}{PE} = \frac{\sigma^2 + f^2}{\sigma^2 - f^2}.$$

From $(D_g\sigma)/(DT) = 0$ (see Eq. (14)) we know that σ is unchanged following the wave packet. So the proportions of Eq. (33) are unchanged following the wave packet. The variation of $|\varphi_0|^2$ can represent the energy variation of wave packet.

It should be pointed out that though the total energy of the whole wave packet is unchanged, the energy of wave packet may be concentrated on a local area and affect weather. From Eq. (31) we obtain $(\mathrm{d}E/\mathrm{d}T) = -E\,\nabla\cdot\boldsymbol{C}_g$. When the group velocity is convergent $(\nabla\cdot\boldsymbol{C}_g < 0)$, $\mathrm{d}E/\mathrm{d}T > 0$, the average energy density of wave packet increases. This means that the volume occupied by wave packet shrinks and the local disturbance will be strengthened. Conversely, when the group velocity is divergent $(\nabla\cdot\boldsymbol{C}_g > 0)$, $\mathrm{d}E/\mathrm{d}T < 0$, the average energy density of wave packet decreases, which means that the volume occupied by wave packet expands and the local disturbance will be weakened. In the following section we will discuss the effects of topography on the wave packet energy variation in this sense.

IV. EFFECTS OF TOPOGRAPHY ON PROPAGATION AND VARIATION OF WAVE PACKET ENERGY

From Eqs. (12), (15), (24) and (31) we get

$$\frac{\mathrm{d}x}{\mathrm{d}t} = C_{gX} = \frac{k}{\sigma}\Phi,$$
$$\frac{\mathrm{d}y}{\mathrm{d}t} = C_{gY} = \frac{l}{\sigma}\Phi,$$
$$\frac{\mathrm{d}k}{\mathrm{d}t} = -\frac{(k^2+l^2)}{2\sigma}\frac{\partial\Phi}{\partial X} = \frac{(k^2+l^2)}{2\sigma}\frac{\partial\varphi_B}{\partial X},$$
$$\frac{\mathrm{d}l}{\mathrm{d}t} = -\frac{(k^2+l^2)}{2\sigma}\frac{\partial\Phi}{\partial Y} = \frac{(k^2+l^2)}{2\sigma}\frac{\partial\varphi_B}{\partial Y}, \tag{34}$$
$$\frac{\mathrm{d}E}{\mathrm{d}T} = -E\,\nabla\cdot\boldsymbol{C}_g,$$
$$\frac{D_g\alpha}{DT} = \frac{f}{2\sigma^2}\left(l\frac{\partial\varphi_B}{\partial X} - k\frac{\partial\varphi_B}{\partial Y}\right),$$

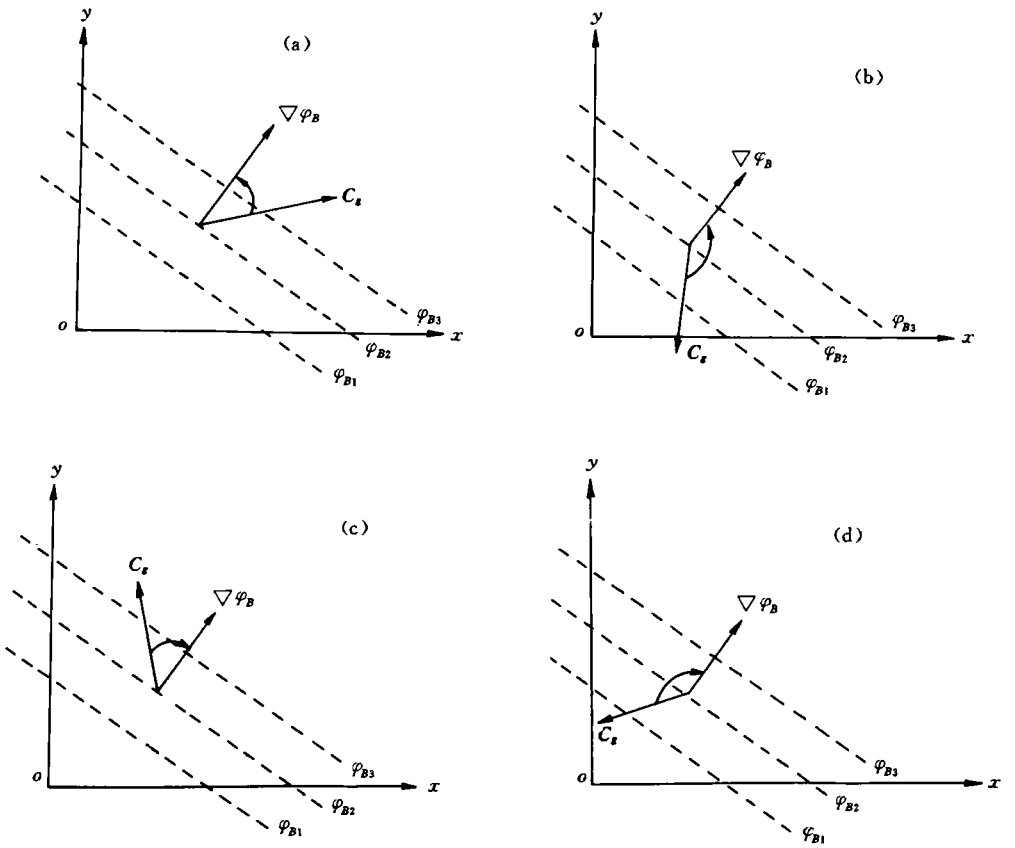

Fig. 1. The variations in different directions in which the wave packet propagates over the topography. Dashed lines show the contours of the topography. (a), (b), (c) and (d) show the cases of different angles between $\boldsymbol{C}_g$ and $\nabla\varphi_B$ respectively.

where $\sigma^2 = f^2 + (k^2+l^2)\Phi$, $\boldsymbol{C}_g = C_{gX}\boldsymbol{i} + C_{gY}\boldsymbol{j}$, $\Phi = g^* H_0 - \varphi_B$. Since the aim to deduce the approximate equations has been reached, it is unnecessary to distinguish the slow and fast variables now. So the variable form of physical coordinate has been taken. According to Eq. (34), the propagation, variation of energy density, the phase of wave envelope and the scales of wave packet can be calculated. When the topography is prescribed as $h_B = h_B(x, y)$, the fluid depth H_0 and the reduced gravity g^* are specified, the initial conditions are given as $x=x_0$, $y=y_0$, $k=k_0$, $l=l_0$, $E=E_0$ and $\alpha=\alpha_0$. We can calculate x, y, k, l, E and α at any time. Before practical calculation is performed we may discuss Eq. (34) qualitatively. From the third and the fourth equations of Eq. (34) we can obtain

$$\frac{\mathrm{d}}{\mathrm{d}t}(k^2+l^2) = -\frac{(k^2+l^2)}{\Phi}\boldsymbol{C}_g \cdot \nabla\Phi = \frac{(k^2+l^2)}{\Phi}\boldsymbol{C}_g \cdot \nabla\varphi_B, \tag{35}$$

when $\boldsymbol{C}_g \cdot \nabla\varphi_B > 0$, $\mathrm{d}/\mathrm{d}t\ (k^2+l^2) > 0$, i. e. the wave packet propagates towards the higher elevation area of the topography, the total wavenumber increases and the wavelength shortens. Conversely, when $\boldsymbol{C}_g \cdot \nabla\varphi_B < 0$, $\mathrm{d}/\mathrm{d}t\ (k^2+l^2) < 0$, i. e. when the wave packet propagates towards the lower elevation area of the topography, the total wavenumber decreases and the wavelength stretches.

Let β be the angle between x-axis and wave ray path, then $\mathrm{tg}\beta = C_{gY}/C_{gX} = l/k$, see Fig. 1. Again according to the third and the fourth equations of Eq. (34) we get

$$\frac{\mathrm{d}\beta}{\mathrm{d}t} = -\boldsymbol{k}\cdot(\boldsymbol{C}_g \times \nabla\varphi/(2\Phi) = \boldsymbol{k}\cdot(\boldsymbol{C}_g \times \nabla\varphi_B)/(2\Phi), \tag{36}$$

where $\boldsymbol{k}$ is unit vector in z direction. Eq. (36) may help us determine the direction of wave packet propagating over a topography. From Fig. 1 and Eq. (36) we see that if the angle between $\boldsymbol{C}_g$ and $\nabla\varphi_B$ is not equal to zero or 180° ($\boldsymbol{C}_g \times \nabla\varphi_B \neq 0$), then $\mathrm{d}\beta/\mathrm{d}t \neq 0$. If $(\boldsymbol{C}_g \times \nabla\varphi_B) > 0$, then $\mathrm{d}\beta/\mathrm{d}t > 0$, and β will increase. The direction of wave packet propagation will curve counterclockwise to satisfy $\boldsymbol{C}_g \times \nabla\varphi_B = 0$. If $(\boldsymbol{C}_g \times \nabla\varphi_B) < 0$, then $\mathrm{d}\beta/\mathrm{d}t < 0$ and β will decrease. The direction of wave packet propagation will curve clockwise to satisfy $\boldsymbol{C}_g \times \nabla\varphi_B = 0$. This process surely happens in the case of simple topography with constant slope. But if the slope is variable, i. e. $\nabla\varphi_B$ is variable, the ray path will be complicated. The ordinary differential equations (34) must be calculated to determine the ray path. Eq. (34) could be solved with Runge-Kutta method. According to the scale analysis of Wu (1994), for the internal inertia gravity waves, $g^* H_0 \sim 10^2 - 10^3\ \mathrm{m^2/s^2}$, $g^* = g\ (\rho_2 - \rho_1)/\rho_1 \sim 1\ \mathrm{m/s^2}$, hence $H_0 \sim 10^2 - 10^3$ m. This magnitude is one order smaller than the depth scale of external gravity waves in the atmosphere. To make the WKBJ analysis valid, the slope scale of topography is taken to be 10^{-3}. In the following calculation we suppose $H_0 = 10^3$ m, $f = 10^{-4}\ \mathrm{s^{-1}}$, $|\varphi_0| = 1\ \mathrm{m^2/s^2}$, $\alpha_0 = 0$, and x_0, y_0, k_0, l_0 will be given in the following. Note that $k = 2\pi/LX$, $l = 2\pi/LY$, so if we have LX and LY, the k and l can be got easily.

Test 1 Assume $h_B(x, y) = 10^{-3}x$ (m), i. e. $h_B(x, y)$ is a linear function of x, and $(x_0, y_0) = (0, 0)$. From Table 1 LX_0 and LY_0 can be obtain.

Table 1. Initial Wavelengths in x and y Directions for Test 1

Number	1	2	3	4	5	6	7	8	9	10
LX_0 (km)	1000	500	300	200	150	100	100	100	100	100
LY_0 (km)	100	100	100	100	100	150	200	300	500	1000

Figure 2 shows that the direction of $\boldsymbol{C}_g$ tends to be perpendicular to the contours of topography, no matter what the initial direction of wave packet propagation is. And along with the propagation of the wave packet the magnitude of $\boldsymbol{C}_g$ gradually decreases. As a matter of fact, under the condition of $h_B(x, y) = 10^{-3}x$ from Eq. (34) we obtain

$$\begin{aligned} \frac{\mathrm{d}k}{\mathrm{d}t} &= 10^{-3}\frac{(k^2 + l^2)}{2\sigma}, \\ \frac{\mathrm{d}l}{\mathrm{d}t} &= 0, \end{aligned} \tag{37}$$

so k is changed with the wave packet propagation but l is constant. And also according to Eq. (34) we have

$$\frac{\mathrm{d}k}{\mathrm{d}x} = \frac{\frac{\mathrm{d}k}{\mathrm{d}t}}{\frac{\mathrm{d}x}{\mathrm{d}t}} = -\frac{(k^2 + l^2)}{2k}\frac{10^{-3}}{(H_0 - 10^{-3}x)}. \tag{38}$$

The solution of Eq. (38) is

$$k^2 = (k_0^2 + l_0^2)\left(\frac{H_0 - 10^{-3}x_0}{H_0 - 10^{-3}x}\right) + l_0^2. \tag{39}$$

Therefore k^2 decreases with the increment of x. When $x \to 10^3 H_0$, then $k^2 \to \infty$, meaning that when the wave packet propagates to the higher elevation area the wavelength will be shortened. Because

$$\Phi = H_0 - 10^{-3}x, \qquad C_{gX} = \frac{k}{\sigma}\Phi,$$

$$C_{gY} = \frac{l}{\sigma}\Phi, \qquad \mathrm{tg}\beta = \frac{C_{gY}}{C_{gX}} = \frac{l}{k},$$

when $x \to 10^3 H_0$, then $C_{gX} \to 0$, $C_{gY} \to 0$ and $\mathrm{tg}\beta \to 0$. Therefore, when the wave packet propagates to the higher elevation area of topography, the propagation direction of the wave packet will be perpendicular to the contours of topography, i. e. parallel to the x-axis. The time that the wave packet propagates from x_0 to $10^3 H_0$ is

$$t = \lim_{x \to 10^3 H_0} \frac{(x - x_0)}{C_{gX}} = \infty.$$

Calculation has also shown that when $\nabla \cdot (\boldsymbol{C_g}) < 0$, $DE/DT > 0$; therefore, the energy density of wave packet increases along with the propagation to the higher elevation area. According to

$$E = \rho_2 \frac{\sigma^2}{(\sigma^2 - f^2)} \frac{|\varphi_0|^2}{2g^*},$$

σ, ρ_2 and g^* are unchanged following the wave packet, so $|\varphi_0|$ increases as the wave packet propagates to the higher elevation place, i. e. the amplitude of perturbation is amplified. This result is consistent with Mei (1984) where the ray theory of water waves in irrotational fluid has been discussed in detail. There are also many observational facts in ocean. When billow waves approach sea beach, they always turn direction to perpendicular to the beach and then lash at the seashore. In these processes the wavelength of sea waves tends to shorten, the amplitude of sea waves tends to amplify. There should be similar phenomena in the atmosphere when inertia gravity waves propagate to a topography. But it has to be pointed out that the amplitude tends to be infinite when Φ is small enough. In our calculation, when $E \to \infty$ the assumption of small amplitude perturbation is invalid, so the WKBJ method can not be applied in this case. Nonlinear and higher order approximation must be regarded. Besides, during the whole process of wave packet propagation the phase angle of wave envelope changed very little ($< 5°$). So the dispersion of wave envelope is weak, the conclusion that the wave packet propagates at group velocity is a good approximation.

Test 2 Assuming $h_B(x, y) = -10^{-3}x$ (m), i. e. $h_B(x, y)$ is a linear function of x also, the topography decreases with the increment of x. Supposing $(x_0, y_0) = (0, 0)$, LX_0 and LY_0 can be got from Table 2 in which the negative wavelength means the wave propagating in the inverse x direction. It only depends on the coordinate.

Figure 3 shows that although the wave packet propagates towards the lower elevation area at initial stage (rays 1—5), it will change the direction of propagation gradually and at last propagate to higher elevation area of topography, because of the influence of topography on the propagation. The following variation is just the same as that in Test 1 but in an inverse x

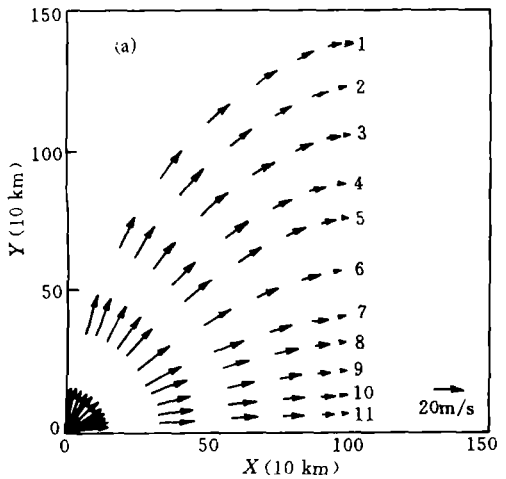

Fig. 2. The rays calculated from Test 1. The direction of arrows indicates the direction of C_g, the length of arrows indicate the magnitude of C_g, and Arabic numerals are consistent with Table 1.

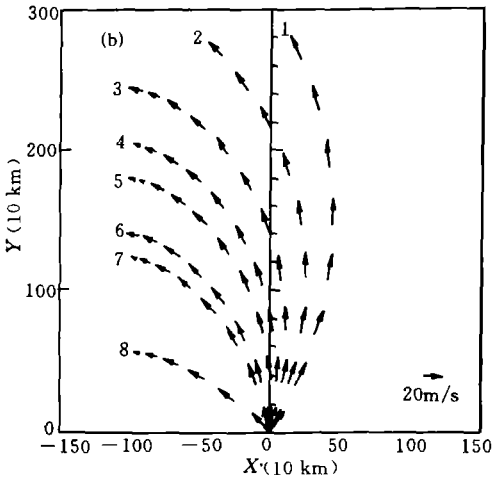

Fig. 3. As in Fig. 2 but for Test 2.

direction, because of assuming $h_B(x, y) = -10^{-3}x$ (m).

Table 2. Initial Wavelengths in x and y Directions for Test 2

Number	1	2	3	4	5	6	7	8
LX_0 (km)	150	200	300	500	1000	−1000	−500	−100
LY_0 (km)	100	100	100	100	100	100	100	100

Test 3 The shape of topography is taken as

$$h_B(x, y) = \frac{10^3}{1 + \left(\frac{x - 1.5 \times 10^6}{5 \times 10^5}\right)^2 + \left(\frac{y - 1.5 \times 10^6}{5 \times 10^5}\right)^2} \text{ (m)},$$

i. e. $h_B(x, y)$ is a round mountain. The top of mountain is at $(1.5\times10^6, 1.5\times10^6)$. The contour of topography is a circle around $(1.5\times10^6, 1.5\times10^6)$. Considering the wave source at (0, 0), LX_0 and LY_0 can be found in Table 3, and the rays calculated from Table 3 are referred to Fig. 4a. Consider three wave sources at (0, 0), $(1.5\times10^6, 0)$ and $(0, 1.5\times10^6)$, respectively, LX_0 and LY_0 can be found in Table 4, and the rays calculated from Table 4 are referred to Fig. 4b.

From Fig. 4 it can be found that the rays have a tendency to propagate to higher elevation area. But not all of them propagate to the top point (150 km, 150 km), which depends on the initial direction and position of the wave packet. Because the round mountain is not a linear function of x and y, so the right side of Eq. (34) is nonlinear. Therefore the behaviour of the rays will be more complicated than those of Tests 1 and 2. The rays 4, 5, 6, 7, 8 in Fig. 4a and rays 1, 2, 3, 6, 9 in Fig. 4b have propagated to the top of topography at last, but other

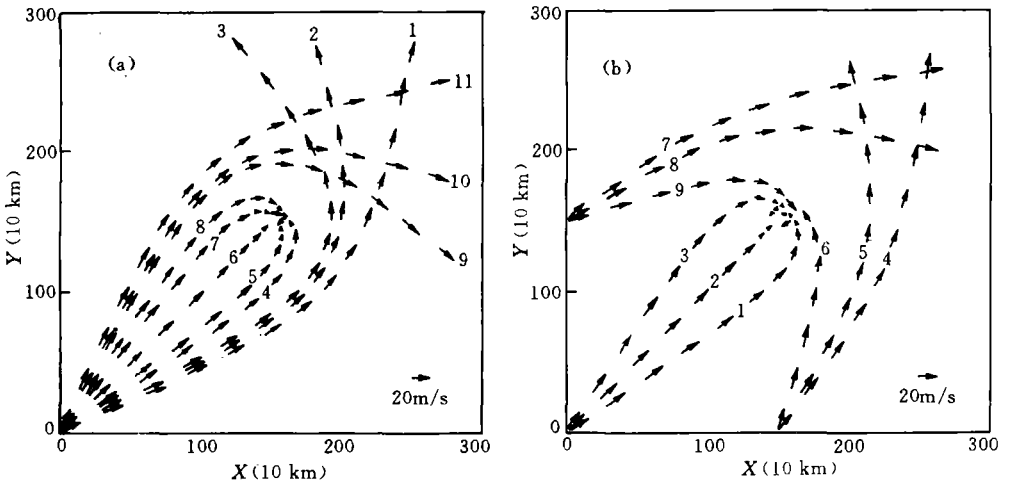

Fig. 4. As in Fig. 2 but for Test 3. (a) One source case. (b) Three source case.

rays have run away, although they have curved and tended to propagate to the higher elevation area of the topography. These rays have intersected on the back of the mountain where they may cause interference. When the two wave packets are superposed in same phase, the amplitude will be amplified; otherwise, reduced.

Table 3. Initial Wavelengths in x and y Directions for Test 3a

Number	1	2	3	4	5	6	7	8	9	10	11
LX_0 (km)	90	100	105	130	150	150	200	200	200	200	200
LY_0 (km)	200	200	200	200	200	150	150	130	105	100	90

Table 4. Initial Wavelengths in x and y Directions and Initial Wave Packet Positions for Test 3b

(x_0, y_0)	(0 km, 0 km)			(150 km, 0 km)			(150 km, 0 km)		
Number	1	2	3	4	5	6	7	8	9
LX_0 (km)	100	150	150	200	250	500	150	150	150
LY_0 (km)	150	150	100	150	150	150	200	250	500

The calculation has shown that the amplitude of waves grows when the wave packet propagates to higher elevation area, while the wave packet propagates to a lower elevation area the amplitude of waves decays. Due to the effects of round topography the wave energy will concentrate on the top of the mountain to some extent.

Wang and Zhang (1992) have discussed the effect of stratification on the propagation and development of inertia gravity waves. Comparing the effects of topography with those of stratification we can found that the topography is quite similar to the small stratification area. Inertia gravity waves have a tendency to propagate to the area of small stability of stratification. Therefore in practical analysis of the effects of inertia gravity waves on the

convection and storm rainfall the internal structure of atmospheric system (including stratification, basic flow structure, etc.) and external factors, such as topography and diabatic heating and so on, must be taken into consideration.

From the above analysis and Figs. 2, 3 and 4, we may have following conclusions. When inertia gravity waves propagate to the higher elevation area of topography, $|\boldsymbol{C}_g|$ decreases; on the contrary, when inertia gravity waves propagate away from the higher elevation area $|\boldsymbol{C}_g|$ increases. The former corresponds to $\nabla \cdot \boldsymbol{C}_g < 0$ and $DE/DT > 0$, the amplitude of waves tends to increase; the latter corresponds to $\nabla \cdot \boldsymbol{C}_g > 0$ and $DE/DT < 0$, the amplitude of waves tends to decrease. The result turns out to be the contrary to Wu' s (1994). This is because Wu made such a coordinate transform that affected his conclusions. As a result, our conclusions are rather correct.

V. SUMMARY

In this paper we have discussed the effects of topography on the propagation and development of inertia gravity waves by using WKBJ method. The equations describing the wave ray path and the wave actions have been obtained. The effects of topography on the inertia gravity waves have been investigated. It has been found out that the inertia gravity waves have a tendency to propagate to higher area of topography. When the inertia gravity waves propagate to a higher elevation area their amplitudes tend to amplify, and vice versa. These principles have meanings for the inertia gravity waves in the lower atmosphere. There are more convections in the mountainous area. In some sense this is due to the fact that there are more inertia gravity wave activities in these areas. It is believed that there are some relationships between inertia gravity wave activities and convections there.

It has to be pointed out that though the wave packet representation of disturbances is very simple and clear in geometric picture, and the WKBJ method can give us the excellent result about the varying coefficient equations, the WKBJ method introduces certain approximation to the original equations, hence such conclusions might be only approximately valid, especially for the wave packet whose amplitude increases to certain extent, so more accurate analysis is needed.

REFERENCES

Chao Jiping (1980), Inertia gravity waves in non-uniform stratified atmosphere and their tentative application in the prediction of storm rainfall. *Sci. Atmos. Sin.*, **4**: 230—235 (in Chinese).

He Haiyan (1989), Internal inertia gravity waves in a non-uniform stratified atmosphere and their role in initiating convection. *J. Trop. Meteor.*, **5**: 8—15 (in Chinese).

Liu Shikuo and Liu Shida (1987), Wave action and stability of internal inertia gravity waves in geophysical fluid. *Sci. Atmos. Sin.*, **11**: 12—21 (in Chinese).

Lu Keli (1986), Effects of topography on the stability of inertia gravity waves on the low level geostrophic flow. *Sci. Atmos. Sin.*, **10**: 220— 224 (in Chinese).

Mei Qiangzhong (1984), *Water Wave Dynamics*. Science Press, Beijing, pp. 338 (in Chinese).

Sun Litan and Zhao Ruixing (1989), On the symmetric development of mesoscale disturbances. *Acta Meteor. Sin.*, **47**: 394—401 (in Chinese).

Wang Donghai and Zhou Xiaoping (1994). Development of transversal wave mesoscale disturbances in the baroclinic atmosphere. *Sci. Atmos. Sin.*, **18**: 61 —71 (in Chinese).

Wang Xingbao and Zhang Weihuan (1992). The influence of low level jet stream and non-uniform stratification on the propagation and development of inertia gravity waves. *J. Trop. Meteor.*, **8**: 323 —333 (in Chinese).

Wang Xingbao and Zhang Weihuan (1993). Development of mesoscale and microscale disturbances superimposed on three-dimensional non-uniform flow. *Science in China*. (Series B) **36**: 1117—1130.

Wu Chisheng (1990). Development of inertia gravity waves in stratified atmosphere. *Sci. Atmos. Sin.*, **14**: 379—383 (in Chinese).

Wu Chisheng (1994). Effect of topography on the development of inertia gravity waves. *Sci. Atmos. Sin.*, **18**: 81—88 (in Chinese).